

CarboNet: A Finite-Time Combustion-Tolerant Compartmental Network for Tropospheric Carbon Control

Federico Zocco¹, Wassim M. Haddad², and Monica Malvezzi¹

Abstract—While governments and international organizations have set the net-zero target to prevent a climate event horizon, practical solutions are lacking mainly because of the impracticability to completely replace combustion processes. Hence, in this paper, we first design a compartmental network whose states must remain in the nonnegative orthant for physical consistency and in which the carbon dioxide emissions result from the combustion of diesel in vehicles and gas in house heaters. Then, we designed both full-state and output-feedback linear-quadratic regulators of the compartmental network to bring the mass of carbon dioxide to the pre-industrial era, which is reached in approximately 25 and 60 days, respectively. The output feedback tolerates for 6 days the combustion taking place in 5,000 vehicles and in 10,000 house heating systems, it meets the net-zero target, and it nullifies the extraction of finite natural resources. The tropospheric temperature with closed-loop reaches the equilibrium at 133 °C after 16.4 years; while such an high value requires to further investigate with climate experts the model of the dynamics of the temperature, this work is a first step in designing optimal network control systems for climate stability. Source code is publicly available¹.

Index Terms—Circular control, circular economy, climate control.

I. INTRODUCTION

While governments and international organizations are adopting measures to prevent a climate event horizon, the temperature anomaly with respect to the pre-industrial era keeps increasing as recorded by NASA [1]. The main cause of this phenomenon are the emissions of greenhouse gases, especially carbon dioxide [2]. Carbon dioxide emissions result from combustion processes that, despite the enormous international effort to adopt combustion-free energy and transportation systems such as wind turbines and electric vehicles, they remain the backbone of our economy. Indeed, the share of primary energy consumption from fossil fuels in 2024 was approximately 73% in Europe and UK and 80% in China and United States [3], while the share of electric cars in use in 2024 was 4.7% in Europe, 6.4% in UK, 11% in China, and 2.7% in United States [4].

To date, the leading control community has not yet contributed significantly to Earth's climate control as visible

by searching for IEEE journal publications: as of 30 July 2025, the first author found only the works of Cavarro [5], Khargonekar *et al.* [6], and De Nardi *et al.* [7]. A recent tutorial on control theory for climate science was recently carried out by Elsherif and Taha [8], which highlights the lack of contributions from the control engineering community to Earth's climate stabilization. Recently, Zocco *et al.* [9] began tackling carbon regulation as a network problem combining nonlinear control and reinforcement learning.

In this context, this paper makes the following contributions.

- Designed a compartmental network modeling the carbon emissions and the fuel consumption of a tunable number of vehicles and house heaters.
- Designed full-state and output feedback linear-quadratic regulators of the network to bring the carbon dioxide in a target urban area to the desired pre-industrial level. While carbon control has been already addressed in Zocco *et al.* [9] as a network control problem, this is the first paper where the control is centralized instead of distributed at different nodes.
- Investigated the nonlinear dynamics of the tropospheric temperature in the target urban area when the network is in closed-loop.
- Measured the circularity of the network to both assess the consumption of natural resources and to insert the net-zero problem within the broader context of a circular economy.

The following notation is adopted throughout the paper: bold lower-case and capital letters are used for vectors and matrices, respectively; the set of nonnegative real numbers is indicated as \mathbb{R}_+ , a vector $\mathbf{x} \in \mathbb{R}^n$ with all nonnegative components is indicated as $\mathbf{x} \geq 0$ or, equivalently, as $\mathbf{x} \in \mathbb{R}_+^n$; similarly, a time-variant vector $\mathbf{x}(t)$ with all nonnegative components for all time is indicated as $\mathbf{x}(t) \in \mathbb{R}_+^n$.

The remaining of the paper is organized as follows. Section II discusses the related work, then Section III covers the framework of linear-quadratic regulator designs along with the definition of the key variables we aim to regulate; subsequently, numerical examples and the case of CO₂ control are detailed in Section IV with full-state feedback and in Section V with output feedback; finally, Section VI concludes.

¹F. Zocco and M. Malvezzi are with the Department of Information Engineering and Mathematics, University of Siena, 53100 Siena, Italy federico.zocco.fz@gmail.com monica.malvezzi@unisi.it

²W. M. Haddad is with the School of Aerospace Engineering, Georgia Institute of Technology, Atlanta, GA 30332, USA. wassim.haddad@aerospace.gatech.edu

¹<https://github.com/ciroresearch/CarboNet>

II. RELATED WORK

A. Circular Economy and Net Zero

The net-zero target required by the United Nations [10] and the European Commission [11] requires to drastically reduce the carbon dioxide emissions. Net-zero, essentially, means that the amount of CO₂ entering the atmosphere is equal to the amount that is removed from it [12].

The circular economy paradigm is gaining attention as a solution to decouple economic growth from sustainable use of natural resources [13]. The practices of a circular economy are, for example, reduce the material demand, reuse material for as long as possible, and repair products [14], [15]. These practices can reduce the carbon dioxide emissions because replacing the raw material extraction, transportation, and manufacturing with the less energy-intensive repair and reuse of functioning product parts and materials [16]–[18]. Hence, increasing circularity helps to meet the net-zero target.

The *circulation* of tropospheric carbon dioxide can further help to meet the net zero target mentioned earlier since carbon circulation yields a removal of carbon from the troposphere. Furthermore, carbon can be *reused* through photosynthesis if plants are used for carbon sequestration as discussed in Section II-B [19]–[21]. In this paper, we increase the circularity of tropospheric carbon dioxide via properly controlled carbon-capture systems.

B. Carbon Capture Systems

An intuitive approach to reduce the concentration of carbon dioxide in the troposphere is removing it. To this aim, different types of technologies are proposed in the literature. Rubin *et al.* [22] analyzed three major solutions, i.e., pre-combustion capture, post-combustion capture, and oxy-combustion capture. In power plants, the captured carbon dioxide can be piped off-shore or injected in underground locations with proper geological properties [23]. The storage of carbon dioxide in fractured rocks was investigated by Romano *et al.* [24].

Nature-based solutions to carbon capture also exist and are divided into two macro-groups. The first group comprises the terrestrial carbon sinks such as forests, urban parks, green roofs, and green facades, while the second group comprises water bodies such as lakes and rivers [21]. In particular, the effectiveness of urban parks in the Italian city of Rome was deepened by Gratani *et al.* [25].

Microalgae are attracting attention because of their high efficiency in carbon absorption compared to other plants and because of their use as biomass at the end of their life [19], [20]. However, most of algal studies are currently limited to laboratory conditions [26].

C. Linear Quadratic Regulators

The linear quadratic regulator (LQR) is a prominent approach for optimal control. It optimizes a positive quadratic cost function and it stabilizes linear time-invariant systems to the origin [27], [28]. Bemporad *et al.* [29] addressed the case of constrained system inputs and outputs, Shi *et al.* [30] developed finite-time horizon LQR with limited controller-system communication, while Maghfiroh *et al.* [31] improved

the LQR performance using particle swarm optimization and the Kalman filter.

Network-control based on LQR was proposed by Jaleel and Shamma [32], in which each agent computes their control actions in real-time, by Duan *et al.* [33] where multi-input linear systems only need to communicate with their neighbors instead of with the whole network, and by Gao *et al.* [34] by leveraging the theory of graphons.

The major limitation of LQRs is that the choice of the weight matrices is often based on empirical considerations and it is problem dependant. To aid in this endeavor, approaches for the tuning of the weight matrices were developed by Chacko *et al.* [35] and by Masti *et al.* [36].

LQRs can be designed not only in the case of access to the whole state, but also in the case of partial knowledge of the state. Solutions to the latter situation were provided by Levine and Athans [37], by Nersesov *et al.* [27], and by Ilka and Murgovski [28].

Examples of applications of the LQR are wind turbine vibration control [38], control of a single-phase inverter [39], and optimal drug delivery [27]. In this paper, we develop both output and full-state feedback LQRs for network-based carbon control.

III. NETWORK, KEY VARIABLES, AND LINEAR-QUADRATIC REGULATORS

This section is divided into three parts: the design of the compartmental network is covered in the first part, then the key sustainability variables to be controlled are introduced, and finally, the LQR design procedure is detailed.

A. Network Design

The compartmental diagram for carbon control considered in this paper is depicted in Fig. 1 and it is based on the formalism of thermodynamical material networks [40]–[44]. Specifically, the green node ($c_{5,5}^5$) is the “CC system”, which is the abbreviation for “carbon capture system”. Its role is to remove the CO₂ from the red node ($c_{1,1}^1$), which indicates the urban area whose carbon dioxide we aim to regulate via the control laws covered in Section III. The tropospheric CO₂ in the urban area is increased by two types of sources: by n_q vehicles with internal-combustion engines ($c_{2,2}^2$) and by n_h heaters ($c_{3,3}^3$); the sources of carbon take and burn the fuel from the natural reserve of oil or gas ($c_{6,6}^6$). The urban area exchanges carbon with the surrounding area indicated with $c_{4,4}^4$. Overall, the system has the four states $x_i(t)$ indicated in blue in Fig. 1, with $i \in \{1, 2, 3, 4\}$, and the control signal $u(t)$ indicated in orange. The states $x_1(t)$ and $x_4(t)$ are masses of CO₂ in the troposphere, while the states $x_2(t)$ and $x_3(t)$ are masses of fuel converted into CO₂ via combustion to move the n_q vehicles (in $c_{2,2}^2$) or to heat-up the n_h buildings (in $c_{3,3}^3$). The system in Fig. 1 can be represented as the thermodynamical material network [40]–[44]

$$\mathcal{N}_c = \{c_{1,1}^1, c_{2,2}^2, c_{3,3}^3, c_{4,4}^4, c_{5,5}^5, c_{6,6}^6, c_{2,1}^7, c_{3,1}^8, c_{4,1}^9, c_{1,4}^{10}, c_{1,5}^{11}, c_{2,4}^{12}, c_{3,4}^{13}, c_{6,2}^{14}, c_{6,3}^{15}\}. \quad (1)$$

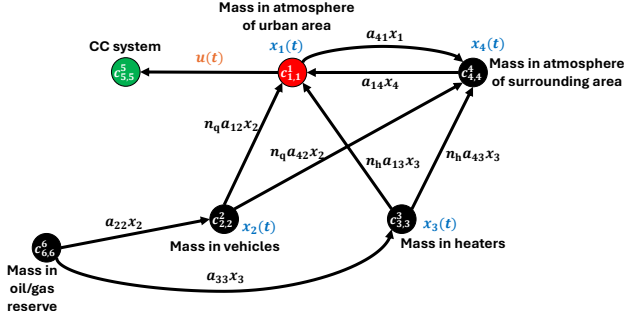


Fig. 1. Compartmental diagram of the system for tropospheric carbon regulation. It can be represented as the set of compartments \mathcal{N}_c (1).

The arcs (i.e., the arrows) in the compartmental diagram indicate the mass flow rates between the compartments, while their weights (i.e., their magnitudes) result from the product between a state $x_i(t)$ of the compartment $c_{i,i}^i$ and a rate constant $a_{k,s} \geq 0$, where for the pair (k, s) it holds that

$$(k, s) = \begin{cases} \begin{cases} k \text{ of the arc head} & \text{if head and tail} \\ c_{k,k}^k \text{ and } s \text{ of the arc} & \text{have states } x_k(t) \\ \text{tail } c_{s,s}^s, & \text{and } x_s(t), \text{ respectively;} \end{cases} \\ k = s, & \text{if at least one between the arc tail } k \\ & \text{or the arc head } s \text{ is not associated with a state.} \end{cases} \quad (2)$$

With the network (1), it holds that the number of compartments, the number of nodes, and the number of arcs are $n_c = 15$, $n_v = 6$, and $n_a = 9$, respectively.

Thus, the vector state is $\mathbf{x}(t) = [x_1(t), x_2(t), x_3(t), x_4(t)]^\top \in \mathbb{R}_+^4$, with the states indicated in Fig. 1, and the control input $u(t) \in \mathbb{R}$. It holds that $\mathbf{x}(t) \geq 0$, while $u(t) < 0$ indicates that the flow has a direction opposite to the one in Fig. 1. The application of the principle of mass balance to the continuous-time system in Fig. 1 yields the following linear ordinary differential equations:

$$\dot{x}_1(t) = -a_{41}x_1(t) + a_{14}x_4(t) + n_h a_{13}x_3(t) + n_q a_{12}x_2(t) - u(t), \quad x_1(0) = x_{10}, \quad t \geq 0, \quad (3)$$

$$\dot{x}_2(t) = a_{22}x_2(t) - n_q a_{12}x_2(t) - n_q a_{42}x_2(t), \quad x_2(0) = x_{20}, \quad (4)$$

$$\dot{x}_3(t) = a_{33}x_3(t) - n_h a_{13}x_3(t) - n_h a_{43}x_3(t), \quad x_3(0) = x_{30}, \quad (5)$$

$$\dot{x}_4(t) = a_{41}x_1(t) - a_{14}x_4(t) + n_q a_{42}x_2(t) + n_h a_{43}x_3(t), \quad x_4(0) = x_{40}. \quad (6)$$

From (3)-(6), we have that the state-space matrix form of the network in Fig. 1 is

$$\dot{\mathbf{x}}(t) = \mathbf{A}\mathbf{x}(t) + \mathbf{B}u(t), \quad \mathbf{x}(0) = \mathbf{x}_0, \quad t \geq 0, \quad (7)$$

$$\mathbf{y}(t) = \mathbf{C}\mathbf{x}(t), \quad (8)$$

where $\mathbf{x}(t) \in \mathbb{R}_+^4$, $t \geq 0$, $\mathbf{A} \in \mathbb{R}^{4 \times 4}$, $\mathbf{B} \in \mathbb{R}^4$, $u(t) \in \mathbb{R}$, $\mathbf{y}(t) \in \mathbb{R}_+^l$, $\mathbf{C} \in \mathbb{R}^{l \times 4}$, and

$$\mathbf{A} = \begin{bmatrix} -a_{41} & n_q a_{12} & n_h a_{13} & a_{14} \\ 0 & \theta_1 & 0 & 0 \\ 0 & 0 & \theta_2 & 0 \\ a_{41} & n_q a_{42} & n_h a_{43} & -a_{14} \end{bmatrix}, \quad \mathbf{B} = \begin{bmatrix} -1 \\ 0 \\ 0 \\ 0 \end{bmatrix}, \quad (9)$$

where $\theta_1 = -n_q(a_{12} + a_{42}) + a_{22}$ and $\theta_2 = -n_h(a_{13} + a_{43}) + a_{33}$. The dimension l is the number of measured states. In Section III-C we will cover the case of full-state feedback (i.e., $l = n = 4$), while Section III-D will cover the case of output feedback (i.e., $l < n = 4$).

B. Dynamics of Key Variables

Throughout the paper, the variables depicting the dynamics of the climate and the natural resources are referred to as “key variables”. The key variables we aim to regulate are: (1) the circularity of carbon dioxide; and (2) the mean tropospheric temperature. As we will show, circularity quantifies two sustainability factors: first, the intensity of use of non-renewable resources; and second, the extent to which the system is close to the *net-zero target* [12] requested by organizations such as the European Commission [11] and the United Nations [10]. In parallel, the mean tropospheric temperature is the main variable affecting climate change; the maximum temperature increase above the pre-industrial era was set to 1.5 °C in the Paris Agreement when it entered into force on 4 November 2016 [45].

1) *Circularity of CO₂*: The dynamics of the *instantaneous circularity*, namely, $\lambda(t)$, is given after the following definition.

Definition 1 ([42]): A mass or flow is *finite-time sustainable* if either it exits a nonrenewable reservoir or it enters a landfill, an incinerator, or the natural environment as a pollutant.

Thus, the *instantaneous circularity* is [42]

$$\lambda(\mathcal{N}; t) = -(\Delta \mu_{fb} \bar{m}_{fb}(t) + \dot{\bar{m}}_{fc}(t)). \quad (10)$$

In (10), \mathcal{N} is a thermodynamical material network [40]–[44], $\bar{m}_{fb}(t)$ is the *net* finite-time sustainable mass transported in batches (e.g., solids transported on trucks) and $\dot{\bar{m}}_{fc}(t)$ is the *net* finite-time sustainable flow transported continuously (e.g., fluids transported through pipes). The quantity

$$\bar{m}_{fb}(t) = c_{fb} m_{fb}(t) \quad (11)$$

is the *weighted* $m_{fb}(t)$, where $c_{fb} \in (0, 1]$ is the criticality coefficient of the material indicating to what extent the material is critical (e.g., high value for a critical raw material [46]), and where $\mu_{fb} \geq 1$ takes into account how many batches of finite-time sustainable materials are disposed of while they are still *functional* (i.e., disposing of faulty parts is better than disposing of working parts). Similarly, $\bar{m}_{fc}(t) = c_{fc} \dot{m}_{fc}(t)$ is the *weighted* $\dot{m}_{fc}(t)$, where $c_{fc} \in [1, +\infty)$ is the criticality coefficient of the finite-time sustainable material transported continuously. Finally, $\Delta > 0$ is a constant with the unit of a frequency introduced as a multiplying factor in order to convert the mass $\bar{m}_{fb}(t)$ into a flow, and hence, to make the sum with $\bar{m}_{fc}(t)$ physically consistent. The choice of Δ

is arbitrary, but its value must be kept the same for any calculation of $\lambda(\mathcal{N}; t)$ in order to make comparisons. Thus, $\lambda(\mathcal{N}; t) \in (-\infty, +\infty)$ and the circularity problem can be stated as

$$\mathcal{N}^* = \arg \max \lambda(\mathcal{N}; t). \quad (12)$$

For the case of \mathcal{N}_c in Fig. 1, it holds that $m_{fb}(t) = 0$. With $c_{fc} = 1$ due to the high criticality of tropospheric CO_2 , the instantaneous circularity (10) yields

$$\lambda_c(\mathcal{N}_c; t) = -\dot{m}_{fc}(t) = -(\phi_1(t) + \phi_{nz}(t)), \quad (13)$$

where

$$\phi_1(t) = a_{22}x_2(t) + a_{33}x_3(t), \quad (14)$$

and

$$\begin{aligned} \phi_{nz}(t) = & n_q a_{12}x_2(t) + n_q a_{42}x_2(t) \\ & + n_h a_{13}x_3(t) + n_h a_{43}x_3(t) - u(t). \end{aligned} \quad (15)$$

Note that, in line with Definition 1, $\phi_1(t)$ takes into account the material flows extracted from non-renewable reserves (i.e., $c_{6,6}^6$), while $\phi_{nz}(t)$ is the difference between the mass flow rate of CO_2 emitted to the atmosphere (which is considered a pollutant because well beyond the natural atmospheric concentrations) and the mass flow rate of CO_2 removed by the carbon-capture system, i.e., $u(t)$. Specifically, $\phi_{nz}(t)$ corresponds to the net-zero target and it is met when

$$\phi_{nz}(t) = 0 \Rightarrow x_1(t) + x_4(t) = \gamma, \quad (16)$$

where $\gamma \in \mathbb{R}_+$ is a constant. The constant γ is the concentration of CO_2 in the considered part of the troposphere, i.e., in the compartments $c_{1,1}^1$ and $c_{4,4}^4$ together, that in the net-zero condition have the total input flow equal to the total output flow (i.e., $u(t)$). Note that the exchange of carbon inside the troposphere, i.e., between $c_{1,1}^1$ and $c_{4,4}^4$, is not constrained in the net-zero target, and hence, in general, $x_1(t)$ and $x_4(t)$ can vary over time even if condition (16) is reached.

2) *Mean Tropospheric Temperature*: A model for the dynamics of the average tropospheric temperature is [8]

$$\dot{T}(t) = \frac{1}{C} [S(1 - \alpha) - \epsilon \sigma T(t)^4], \quad (17)$$

where $T(t)$ [K] is the mean tropospheric temperature, C [$\text{Jm}^{-2}\text{K}^{-1}$] is the effective heat capacity of the Earth, which quantifies how the system is sensitive to energy variations, S [$\text{Js}^{-1}\text{m}^{-2}$] is the average incoming solar energy per unit area, $\alpha \in [0, 1]$ models the fraction of solar energy reflected by the Earth (i.e., the albedo effect), $\sigma = 5.67 \times 10^{-8} \text{ Js}^{-1}\text{m}^{-2}\text{K}^{-4}$ is the Stefan-Boltzmann's constant, and $\epsilon \in [0, 1]$ is the emissivity of Earth, which quantifies how much energy is sent back to space and it is reduced by an increase of the concentration of CO_2 in the troposphere. Thus, the variation of the tropospheric temperature of Earth (17) is affected by two contrasting contributions: the amount of energy entering the troposphere and not reflected back (i.e., the term multiplied by S), and by the outgoing longwave radiation (i.e., $\epsilon \sigma T(t)^4$).

To take into account in (17) of the CO_2 concentration, which is regulated by our control scheme, the emissivity is modeled as

$$\epsilon(t) = \epsilon_n - d_c(t), \quad (18)$$

where

$$d_c(t) = \eta \frac{x_1(t)}{V_1}, \quad (19)$$

ϵ_n is the normal emissivity of a urban area, $d_c(t)$ is the disturbance to the emissivity induced by the carbon dioxide concentration in the target urban area $c_{1,1}^1$, $\eta = 2.36 \times 10^{-4} \text{ km}^3/\text{t}$ is a multiplying factor added to make $d_c(t)$ nondimensional and maintaining $\epsilon(t)$ within the usual range 0.6-1.0 [47], and V_1 is the volume of compartment $c_{1,1}^1$.

C. Full-State Feedback

The control law leveraged in this paper for full-state feedback was proposed in [27] and applied for optimal drug delivery. The analogy between drug delivery and carbon control for climate stability is that the states of the compartments must remain in the nonnegative orthant since they are masses, and hence, negative values are physically inconsistent.

Given that the control input in our network system (Fig. 1 and equations (7)-(9)) is not constrained to be an injection for the regulated compartment (i.e., $c_{1,1}^1$), the controller in [27, Section 6] is not applicable. Thus, we implement the optimal non-zero set-point regulator covered in [27, Section 4] and we set $C = I_n$, where $I_n \in \mathbb{R}^{n \times n}$ is the identity matrix. Specifically, the control input takes the form

$$u(t) = -K(y(t) - Cx_e) + v_e, \quad (20)$$

where $K \in \mathbb{R}^{1 \times l}$ is the controller such that

$$u(t) = -K y(t), \quad (21)$$

and where $v_e \in \mathbb{R}$, $x_e \in \mathbb{R}_+^n$ is an equilibrium for (7), and $x_e = [x_{1e}, x_{2e}, x_{3e}, x_{4e}]^\top$. Thus, the closed-loop system becomes

$$\dot{x}(t) = \hat{A}x(t), \quad x(0) = x_0, \quad t \geq 0, \quad (22)$$

where $\hat{A} = A - BKC$. If

- the pair (A, B) is stabilizable,
- [set-point condition] $\exists v_e \in \mathbb{R} : 0 = Ax_e + Bv_e$, with $x_e \in \mathbb{R}_+^n$ the desired set-point,
- the pair (A, R_1) is observable, with $R_1 \in \mathbb{R}^{n \times n}$ and $R_1 \geq 0$,
- and $\exists P$:

$$0 = A^\top P + PA + R_1 - PSP, \quad (23)$$

with $S = r_2^{-1}BB^\top$ and $r_2 > 0$,

then, the controller $K \in \mathbb{R}^{1 \times l}$:

- guarantees that the closed-loop system (22) is globally asymptotically stable in $x_e \in \mathbb{R}_+^n$;
- it is optimal in the sense that it minimizes the performance functional

$$\begin{aligned} J(x_0, u) = & \frac{1}{2} \int_0^\infty [(x(t) - x_e)^\top R_1 (x(t) - x_e) \\ & + (u(t) - v_e)^\top r_2 (u(t) - v_e) \\ & + 2(x(t) - x_e)^\top N(u(t) - v_e)] dt. \end{aligned} \quad (24)$$

In addition, let $\mathcal{D}_A \subseteq \overline{\mathbb{R}}_+^n$ be the domain of attraction such that $\mathbf{x}(t) \in \mathcal{D}_A \subseteq \overline{\mathbb{R}}_+^n$ for $t \geq 0$ and $\forall \mathbf{x}_0 \in \mathcal{D}_A$ [27]; if $\mathbf{x}_0 \in \mathcal{D}_A$, the controller $\mathbf{K} \in \mathbb{R}^{1 \times l}$ guarantees that $\mathbf{x}(t) \geq 0$, that is, the state trajectories remain in the non-negative orthant of \mathbb{R}^n at all time, which preserves the fundamental property of non-negative states for the closed-loop system (22).

Hence, the procedure to design the controller is as follows.

- 1) Verify that the pair (\mathbf{A}, \mathbf{B}) is stabilizable;
- 2) [set-point condition] $\exists v_e \in \mathbb{R} : 0 = \mathbf{A}\mathbf{x}_e + \mathbf{B}v_e$, with \mathbf{x}_e the desired set-point;
- 3) Choose $\mathbf{R}_1 \geq 0$ such that the pair $(\mathbf{A}, \mathbf{R}_1)$ is observable;
- 4) choose $r_2 > 0$ and find \mathbf{P} by solving the algebraic Riccati's equation (23);
- 5) compute the feedback gain $\mathbf{K} = (1/r_2)\mathbf{B}^\top \mathbf{P}$;
- 6) compute the translated initial conditions as $\tilde{\mathbf{x}}_0 = \mathbf{x}_0 - \mathbf{x}_e$; choose the initial conditions \mathbf{x}_0 such that either $\mathbf{x}_0 \in \mathcal{D}_A$, with \mathcal{D}_A calculated as in [27], or the closed-loop state $\mathbf{x}(t) \geq 0$, which can be verified a posteriori;
- 7) implement the closed-loop system as

$$\dot{\tilde{\mathbf{x}}}(t) = \hat{\mathbf{A}}\tilde{\mathbf{x}}(t), \quad \tilde{\mathbf{x}}(0) = \tilde{\mathbf{x}}_0, \quad t \geq 0, \quad (25)$$

where $\tilde{\mathbf{x}}(t) = \mathbf{x}(t) - \mathbf{x}_e$ is the translated state so that the origin $\mathbf{0}$ corresponds to the desired set-point \mathbf{x}_e ;

- 8) recover the original state as $\mathbf{x}(t) = \tilde{\mathbf{x}}(t) + \mathbf{x}_e$ and the original initial conditions as $\mathbf{x}_0 = \tilde{\mathbf{x}}_0 + \mathbf{x}_e$;
- 9) verify that $\lim_{t \rightarrow \infty} u(t) = v_e$ by computing $u(t)$ as in (20) with $\mathbf{y}(t) = \mathbf{C}(\tilde{\mathbf{x}}(t) + \mathbf{x}_e)$; $u(t) > 0$ indicates that the direction of $u(t)$ is the one considered in (9);
- 10) verify that the closed-loop state $\mathbf{x}(t) \geq 0$; if not, \mathbf{x}_e and/or \mathbf{x}_0 must be changed.

The set-point condition fixes at which state \mathbf{x}_e the closed-loop system is desired to work. After a transitory phase, the states of the closed-loop system converge to the equilibrium \mathbf{x}_e while the control input $u(t)$ converges to the constant value v_e . Now, note that the origin of the dynamical system (3)-(6), i.e., $\mathbf{x}(t) \equiv \mathbf{0}$, is not a desired set-point for our carbon control problem. Specifically, we need to choose $x_{ie}|_{i \in \{1,4\}} \neq 0$ to replicate the real-world conditions, i.e., the masses of CO_2 in the troposphere compartments ($c_{1,1}^1$ and $c_{4,4}^4$) are nonzero. Thus, imposing the set-point condition to the dynamical system (3)-(6) with $x_{ie}|_{i \in \{1,4\}} \neq 0$ yields

$$v_e = -a_{41}x_{1e} + a_{14}x_{4e} + n_h a_{13}x_{3e} + n_q a_{12}x_{2e}, \quad (26)$$

$$0 = (a_{22} - n_q a_{12} - n_q a_{42})x_{2e}, \quad (27)$$

$$0 = (a_{33} - n_h a_{13} - n_h a_{43})x_{3e}, \quad (28)$$

$$0 = a_{41}x_{1e} - a_{14}x_{4e} + n_q a_{42}x_{2e} + n_h a_{43}x_{3e}. \quad (29)$$

The conditions (27) and (28) require to have $x_{ie}|_{i \in \{2,3\}} = 0$ (i.e., no mass of fuel and gas in vehicles and houses at equilibrium); indeed, if $x_{ie}|_{i \in \{2,3\}} \neq 0$, conditions (27) and (28) yield $\theta_1 = \theta_2 = 0$, which makes the pair (\mathbf{A}, \mathbf{B}) not

stabilizable. With $x_{ie}|_{i \in \{2,3\}} = 0$, equations (26)-(29) become

$$v_e = 0, \quad (30)$$

$$a_{22} \neq n_q(a_{12} + a_{42}), \quad (\text{i.e., } \theta_1 \neq 0) \quad (31)$$

$$a_{33} \neq n_h(a_{13} + a_{43}), \quad (\text{i.e., } \theta_2 \neq 0) \quad (32)$$

$$x_{4e} = \frac{a_{41}}{a_{14}}x_{1e}, \quad (33)$$

with $\mathbf{x}_e = [x_{1e}, 0, 0, x_{4e}]^\top$.

D. Output Feedback

In practice, it is often unfeasible to measure the full state of a system as required for full-state feedback. When the full state is not measured, the LQR design problem is referred to as “output feedback”. In this section, we cover the case in which only the mass of CO_2 in the target area is known, i.e., in the compartment $c_{1,1}^1$. Thus,

$$\mathbf{y}(t) = \mathbf{C}\mathbf{x}(t), \quad \mathbf{C} = [1, 0, 0, 0]. \quad (34)$$

When $\mathbf{C} \neq \mathbf{I}_n$, finding an optimal stabilizing feedback gain \mathbf{K} is more complex and it requires to iteratively solve one or more algebraic Riccati equations. In this paper, we use the algorithms developed by Ilka and Murgovski [28]. The procedure we followed for the LQR design in the case of output feedback can be summarized as follows, with the conditions for stabilizability detailed in [28, Theorem 1]:

- 1) verify that the pair (\mathbf{A}, \mathbf{B}) is stabilizable (e.g., through the PBH test);
- 2) verify that the pair (\mathbf{A}, \mathbf{C}) is detectable (e.g., through the PBH test);
- 3) verify that the weight matrices in the performance functional (24) satisfy

$$\begin{bmatrix} \mathbf{R}_1 & \mathbf{N} \\ \mathbf{N}^\top & r_2 \end{bmatrix} \geq 0, \quad r_2 > 0, \quad (35)$$

with $\mathbf{R}_1 \in \mathbb{R}^{n \times n}$, $\mathbf{N} \in \mathbb{R}^{n \times 1}$, and $r_2 \in \mathbb{R}$;

- 4) run an algorithm of [28] to find a feedback gain $\mathbf{K} \in \mathbb{R}^{1 \times l}$ and an approximate solution $\mathbf{P} \in \mathbb{R}^{n \times n}$ of the algebraic Riccati equation

$$\mathbf{A}^\top \mathbf{P} + \mathbf{P}\mathbf{A} + \mathbf{R}_1 + r_2 \mathbf{G}^\top \mathbf{G} - r_2^{-1}(\mathbf{P}\mathbf{B} + \mathbf{N})(\mathbf{B}^\top \mathbf{P} + \mathbf{N}^\top) = \mathbf{0}, \quad (36)$$

where $\mathbf{G} \in \mathbb{R}^{1 \times n}$ is computed as

$$\mathbf{G} = \mathbf{K}\mathbf{C} - r_2^{-1}(\mathbf{B}^\top \mathbf{P} + \mathbf{N}^\top); \quad (37)$$

- 5) compute $\mathbf{G} \in \mathbb{R}^{1 \times n}$ as in (37);
- 6) check that the equality (36) is satisfied;
- 7) implement the closed-loop system as in (25);
- 8) recover the original state as $\mathbf{x}(t) = \tilde{\mathbf{x}}(t) + \mathbf{x}_e$ and the original initial conditions as $\mathbf{x}_0 = \tilde{\mathbf{x}}_0 + \mathbf{x}_e$;
- 9) verify that $\lim_{t \rightarrow \infty} u(t) = v_e$ by computing $u(t)$ as in (20) with $\mathbf{y}(t) = \mathbf{C}(\tilde{\mathbf{x}}(t) + \mathbf{x}_e)$;
- 10) verify that the closed-loop state $\mathbf{x}(t) \geq 0$; if not, \mathbf{x}_e and/or \mathbf{x}_0 must be changed.

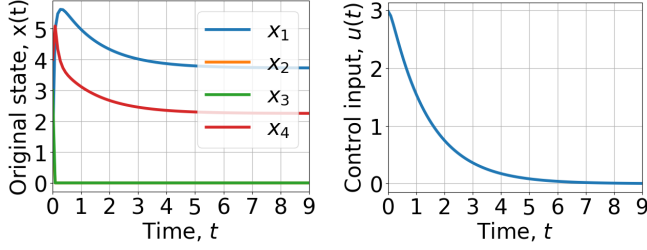


Fig. 2. Closed-loop state and control input with *full-state feedback* and random rate constants $a_{k,s}$.

IV. NUMERICAL STUDIES: FULL-STATE FEEDBACK

This section is divided into two parts. In the first part, we consider random rate constants in the linear system (9) for testing the control scheme. In the second part, we move to consider realistic parameters and address the control of tropospheric carbon (17) and the system circularity (13). For the full-state feedback, we leveraged the Python library of Fuller *et al.* [48].

A. Random Rate Constants

We begin the numerical studies by considering the following state matrix with random rate constants $a_{k,s}$, with $n_q = 15$, and with $n_h = 7$:

$$\mathbf{A} = \begin{bmatrix} -3.41 & 95.82 & 39.62 & 5.63 \\ 0 & -128.85 & 0 & 0 \\ 0 & 0 & -95.20 & 0 \\ 3.41 & 38.57 & 63.91 & -5.63 \end{bmatrix}. \quad (38)$$

Thus, $\theta_1 = -128.85$ and $\theta_2 = -95.20$. The matrix \mathbf{A} has eigenvalues 0, -9.04, -128.85, and -95.20, while the pair (\mathbf{A}, \mathbf{B}) is stabilizable from the Popov–Belevitch–Hautus (PBH) test [49]. The set-point is also set by randomly choosing $x_{1e} = 3.73$ and imposing (30)–(33); thus, $x_e = [3.73, 0, 0, 2.25]^T$. We set $\mathbf{R}_1 = \mathbf{I}_4$, and hence, the pair $(\mathbf{A}, \mathbf{R}_1)$ is observable. The solution of the algebraic Riccati equation with $r_2 = 1$ (23) yields \mathbf{P} , which is then used to compute the feedback gain $\mathbf{K} = [-0.75, -0.76, -0.77, -0.69]$. With testing initial conditions $x_0 = [1, 2, 3, 4]^T$, the closed-loop original state and control input are shown in Fig. 2. The state converges to the desired set-point x_e with the equilibrium input $v_e = 0$. Moreover, $x(t) \geq 0$, which is physically consistent since the states are masses.

B. Case of Tropospheric CO₂

We now consider realistic initial condition and set-point to tackle the control of the concentration of tropospheric carbon. Specifically, we consider the current state of the atmosphere as initial conditions and the pre-industrial condition as the set-point state. In other words, the controller is expected to bring the concentration of CO₂ to the pre-industrial era.

Let x_{i0} be the initial condition of the i -th state. We consider a target urban area with volume $V_1 = 1.18 \text{ km}^3$, which results from the product between the surface of the Italian city of Siena (approximately 118 km^2) and an high of 0.01

TABLE I
RATE CONSTANTS USED IN THE CASE OF TROPOSPHERIC CO₂.

a_{41}	a_{12}	a_{13}	a_{14}	a_{42}	a_{22}	a_{43}	a_{33}
0.2	$0.5/n_q$	$0.5/n_h$	0.1	$0.5/n_q$	0.3	$0.5/n_h$	0.6

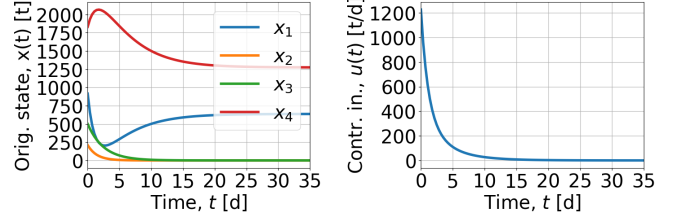


Fig. 3. Closed-loop state and control input with *full-state feedback* for tropospheric CO₂ control.

km. Given that the current concentration of carbon dioxide in the atmosphere is 431 ppm [2], the current mass of carbon inside a volume V_1 is 915.4 tonnes; thus, $x_{10} = 915.4 \text{ t}$. The surrounding area $c_{4,4}^1$ has a volume twice the one of $c_{1,1}^1$, and hence, $x_{40} = 1,830.8 \text{ t}$. To set the initial mass of fuel (diesel) in $c_{2,2}^2$, i.e., x_{20} , we consider $n_q = 5,000$ vehicles with a tank of 50 liters each; this yields 42 kg of diesel per vehicle, and hence, $x_{20} = 210 \text{ t}$. The initial mass of gas inside pipelines and in one house is set as 50 kg, and hence, with the number of houses set as $n_h = 10,000$, we have that $x_{30} = 500 \text{ t}$.

Since the set-point condition corresponds to the pre-industrial era in which the concentration of CO₂ was approximately 300 ppm, we set $x_{1e} = 637.2 \text{ t}$. Assuming the rate coefficients in Table I, we have that $x_{4e} = (a_{41}/a_{14})x_{1e} = 1,274.4 \text{ t}$ (imposition of (33)). Thus, the state matrix becomes

$$\mathbf{A} = \begin{bmatrix} -0.2 & 0.5 & 0.5 & 0.1 \\ 0.0 & -0.7 & 0.0 & 0.0 \\ 0.0 & 0.0 & -0.4 & 0.0 \\ 0.2 & 0.5 & 0.5 & -0.1 \end{bmatrix}, \quad (39)$$

$\theta_1 = -0.7$, and $\theta_2 = -0.4$. The eigenvalues of \mathbf{A} are -0.3, 0, -0.7, and -0.4, while the pair (\mathbf{A}, \mathbf{B}) is stabilizable. By choosing $\mathbf{R}_1 = \mathbf{I}_4$, the pair $(\mathbf{A}, \mathbf{R}_1)$ is observable. With $r_2 = 1$, the optimal gain becomes $\mathbf{K} = [-0.94, -0.67, -0.93, -0.65]$. The response of the closed-loop system to the initial conditions specified previously and the control input are shown in Fig. 3. As visible, the concentration in the pre-industrial era x_{1e} is reached in approximately 25 days. Note that, since $x_{2e} = x_{3e} = 0$, all the mass flow rates converge to zero with the exception of the flows between $c_{1,1}^1$ and $c_{4,4}^1$, i.e., the tropospheric regions are a closed system at equilibrium. This result explains why the paper title specifies that the network is “finite-time combustion-tolerant”: to reach the desired pre-industrial era condition inside the target area, i.e., to reach x_{1e} , this control scheme brings to zero the CO₂ emissions of the n_q vehicles and the n_h houses, i.e., the mass flow rates from $c_{2,2}^2$ and $c_{3,3}^3$ to $c_{1,1}^1$ and $c_{4,4}^1$. Specifically, this full-state control scheme tolerates the combustion taking place in 5,000 vehicles and in 10,000 house heating systems for approximately 6 days, which is the time it needs to bring $x_2(t)$ and $x_3(t)$ to zero.

The dynamics of the key variables are reported in Fig. 4. Initially, circularity $\lambda(t)$ is positive because the extraction of carbon, i.e., $u(t)$, dominates over the other flows; at equilibrium, the extraction of finite natural resources $\phi_1(t)$ reaches zero, and so does the net-zero variable $\phi_{nz}(t)$. In particular, this controller meet the net-zero target (16) by nullifying both the input flows and the output flows of the tropospheric areas $c_{1,1}^1$ and $c_{4,4}^4$. Fig. 4 also shows the dynamics of the tropospheric temperature, for which we set the current atmospheric temperature reported by NASA [1] as the initial condition, i.e., $T(0) = 15.2$ °C. The simulation is obtained for $C = 8 \times 10^8$ J K⁻¹ m⁻², $\alpha = 0.3$, and $S = 1367.6 \times 86400$ J d⁻¹ m⁻² (values taken from [8]). The temperature has a dynamics much slower than that of the states since its first derivative starts to reduce after approximately 2000 days, that is, 5.5 years; *after 16.4 years (6000 days), the temperature reaches the equilibrium value of 133 °C. This value is so high that it requires further investigation with climate experts of the model (17) (result similar to that obtained in [8, Fig. 7]).* Finally, Fig. 4 shows the emissivity $\epsilon(t)$, which is inversely proportional to $x_1(t)$.

Remark: In terms of the implementation of (17) in combination with the closed-loop system, it is worth pointing out that the former is nonlinear, whereas the latter is linear. Thus, we achieved the dynamics of $T(t)$ by numerically integrating the resulting system of five ordinary differential equations with the Python function `scipy.integrate.odeint()`. Coherently with the states $x_i(t)|_{i=1,2,3,4}$, we translated the temperature to the condition in the pre-industrial era, and hence, $\tilde{T}(t) = T(t) - T_e$, with $T_e = 13.9$ °C. However, T_e may not be an equilibrium for (17), which is not required by the control law because the regulator acts on the states $x_i(t)|_{i=1,2,3,4}$, not directly on $T(t)$. The controller affects $T(t)$ indirectly through $\epsilon(t)$, which is a function of $x_1(t)$ in closed loop.

V. NUMERICAL STUDIES: OUTPUT FEEDBACK

This section covers numerical studies in the case of output feedback with the controller design detailed in Section III-D. Similarly to Section IV, first it tests the control with random rate constants $a_{k,s}$, and then, it considers and discusses the case of rate constants set to tackle the control of the tropospheric carbon and the carbon circularity in a target area $c_{1,1}^1$. For the output feedback, we leveraged the MATLAB implementations made available by Ilka and Murgovski [28].

A. Random Rate Constants

We consider the same rate constants of Section IV-A, and hence, the matrix A corresponds to (38). Thus, the pair (A, B) is stabilizable. The PBH test shows also that the pair (A, C) is detectable. Similarly to [28], the weight matrices have been chosen as $R_1 = C^T C$, $r_2 = 1$, and $N = 0$. Thus, the condition (35) is satisfied. By running the Newton's method and the modified Newton's method of [28], we obtained $K = -0.694$ with both algorithms. The two methods returned slightly different P matrices, but the difference between corresponding entries of the two returned P matrices were smaller than 10^{-7} , and hence, both methods

gave approximately the same $G = [0, 0.696, 0.698, 0.618]$. Furthermore, condition (36) was satisfied by both methods since the left-hand side of the equality contained entries smaller than 10^{-7} . The implementation of the closed-loop system (22) with testing initial conditions $x_0 = [1, 2, 3, 4]^T$ and set-point state $x_e = [1, 0, 0, 0.605]^T$ gave the results shown in Fig. 5. The controller stabilizes the translated state to the origin because its goal is to minimize the performance functional (24), while for the original state and control input we have that $\lim_{t \rightarrow \infty} x(t) = x_e$ and $\lim_{t \rightarrow \infty} u(t) = v_e$ (remember that $v_e = 0$ from equation (30)). In addition, for the state in closed loop it holds that $x(t) \geq 0$, which is physically consistent.

B. Case of Tropospheric CO₂

This section addresses the control of tropospheric carbon as in Section IV-B, but designing an output-feedback control. Thus, the state matrix is that in equation (39) and the control design procedure follows that of Section V-A with matrices tuned as $R_1 = C^T C$, $r_2 = 1$, $N = 0$, and $R_1 = I_4$. Hence, the pair (A, B) is stabilizable, the pair (A, C) is detectable, the condition (35) is satisfied, while the Newton's and the modified Newton's methods of [28] yield $K = -0.837$. The two methods returned slightly different P matrices, but the difference between corresponding entries of the two returned P matrices were smaller than 10^{-7} , and hence, both methods gave approximately the same $G = [0, 0.284, 0.357, 0.089]$. Furthermore, condition (36) was satisfied by both methods since the left-hand side of the equality contained entries smaller than 10^{-7} . The implementation of the closed-loop system with the initial and set-point conditions used in Section IV-B gives the results reported in Fig. 6. As visible, *the concentration of CO₂ in the target area reaches the value of the pre-industrial era (i.e., 637.2 tonnes) in approximately 60 days, which is about 35 days slower than the system with full-state control.* The fact that the action of the output-feedback controller is slower than the full-state one is explained by comparing the control inputs: $u(0) \approx 260$ t/d in the former and $u(0) \approx 1200$ t/d in the latter, which is motivated by the fact that the full-state acts on all the four states, whereas the output-feedback only on one state (i.e., $x_1(t)$).

The key variables with output-feedback are shown in Fig. 7. In particular, $\lambda(0)$ is negative in contrast with the case of full-state feedback since, as discussed above, the control input $u(0)$ is more than 4 times smaller. Analogously to the case of full-state feedback, $\lambda(t)$, $\phi_1(t)$, and $\phi_{nz}(t)$ converge to zero, while the tropospheric temperature converges to 133 °C in approximately 16.4 years. In contrast, the emissivity $\epsilon(t)$ has a different response in the full-state setting compared to the output-feedback setting.

VI. CONCLUSION

This paper proposes CarboNet, a network of thermodynamic compartments controlled via LQRs for tropospheric carbon regulation. The controllers effectively reduced the CO₂ concentration to the pre-industrial era level and also met the net-zero target, but they tolerated CO₂ emissions for only 6 days.

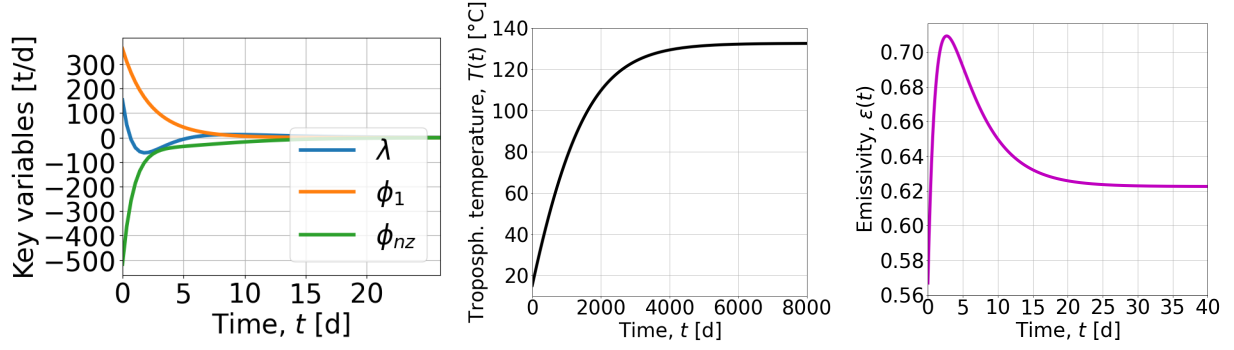


Fig. 4. Key variables with *full-state feedback*: (left) circularity, ϕ_1 , and ϕ_{nz} ; (middle) tropospheric temperature; (right) emissivity.

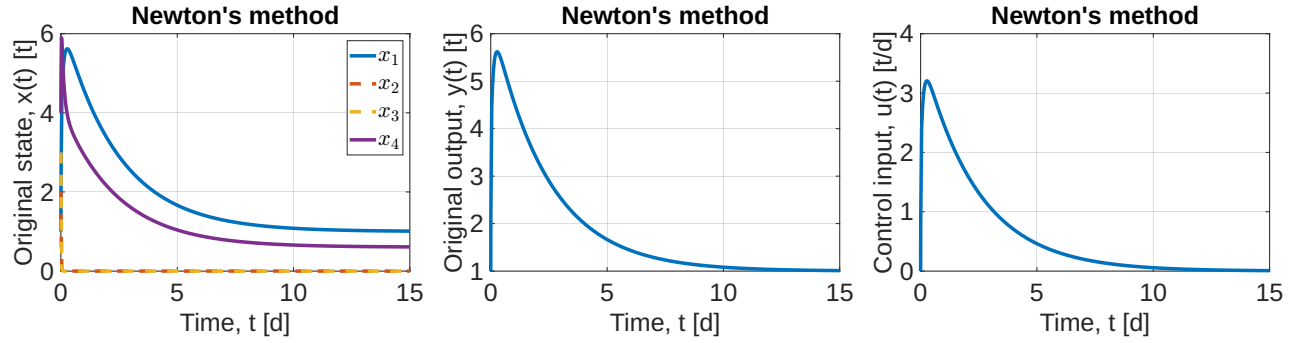


Fig. 5. Closed-loop state, output, and control input with *output-feedback* gain computed via the Newton's method [28] in the case of random rate constants $a_{k,s}$.

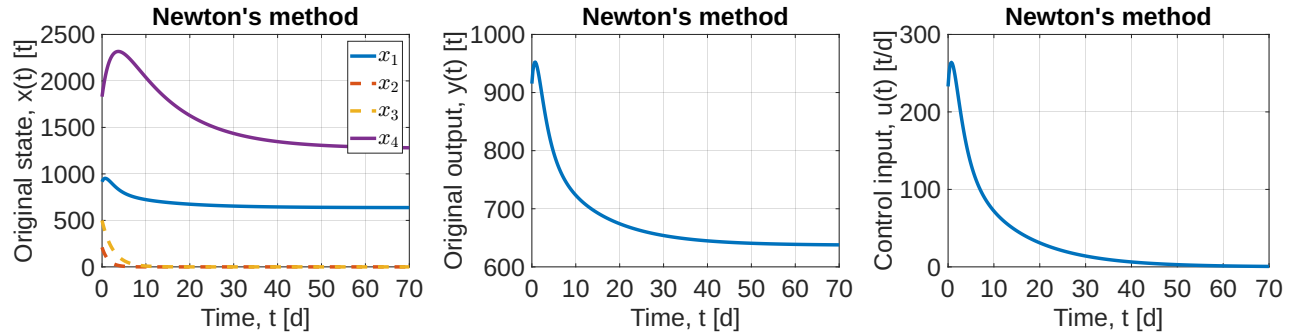


Fig. 6. Closed-loop state, output, and control input with *output-feedback* gain computed via the Newton's method [28] for tropospheric CO_2 control.

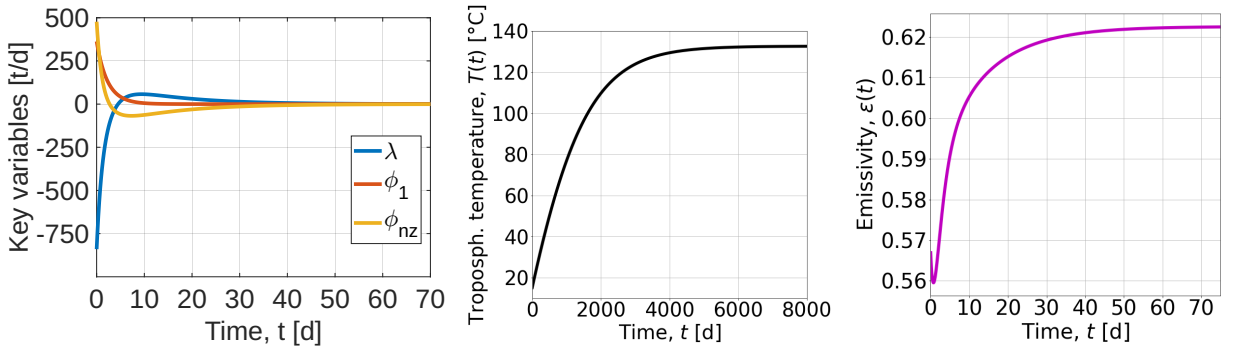


Fig. 7. Key variables with *output feedback*: (left) circularity, ϕ_1 , and ϕ_{nz} ; (middle) tropospheric temperature; (right) emissivity.

The tropospheric temperature stabilizes at 133 °C in 16.4 years. The high of this value suggests to further investigate the temperature model in collaboration with climate experts, which is left as future work along with making the control system able to tolerate the combustion for more than 6 days.

REFERENCES

- [1] National Aeronautics and Space Administration (NASA), “Vital signs – Global temperature,” last access: 25 July 2025. Available at: <https://climate.nasa.gov/vital-signs/global-temperature/>.
- [2] —, “Carbon dioxide,” last access: 25 July 2025. Available at: <https://climate.nasa.gov/vital-signs/carbon-dioxide/?intent=121>.
- [3] Our World in Data, “Share of primary energy consumption that comes from fossil fuels,” last access: 30 July 2025. Available at: https://ourworldindata.org/grapher/fossil-fuels-share-energy?tab=line&country=~USA&mapSelect=~OWID_EUR.
- [4] —, “Share of cars currently in use that are electric,” last access: 30 July 2025. Available at: https://ourworldindata.org/grapher/share-car-stocks-electric?country=OWID_WRL~CHN~USA~OWID_EUR.
- [5] G. Cavarero, “Advocating feedback control for human-Earth system applications,” *IEEE Control Systems Letters*, vol. 8, pp. 1757–1762, 2024.
- [6] P. P. Khargonekar, T. Samad, S. Amin, A. Chakraborty, F. Dabbene, A. Das, M. Fujita, M. Garcia-Sanz, D. F. Gayme, M. Ilić *et al.*, “Climate change mitigation, adaptation, and resilience: Challenges and opportunities for the control systems community,” *IEEE Control Systems Magazine*, vol. 44, no. 3, pp. 33–51, 2024.
- [7] S. De Nardi, C. Carnevale, S. Raccagni, and L. Sangiorgi, “Climate change impact on cereal production in northern Africa: A comprehensive modelling and control approach,” *IEEE Access*, vol. 13, pp. 5534–5550, 2025.
- [8] S. M. Elsherif and A. F. Taha, “Climate science and control engineering: Insights, parallels, and connections,” *arXiv preprint arXiv:2504.21153*, 2025.
- [9] F. Zocco, J. García, and W. M. Haddad, “Circular microalgae-based carbon control for net zero,” *arXiv preprint arXiv:2502.02382*, 2025.
- [10] United Nations, “For a livable climate: Net-zero commitments must be backed by credible action,” last access: 25 July 2025. Available at: <https://www.un.org/en/climatechange/net-zero-coalition>.
- [11] European Commission, “2050 long-term strategy,” last access: 30 July 2025. Available at: https://climate.ec.europa.eu/eu-action/climate-strategies-targets/2050-long-term-strategy_en.
- [12] University of Oxford, “What is net zero?” last access: 25 July 2025. Available at: <https://netzeroclimate.org/what-is-net-zero-2/>.
- [13] A. Alexander, S. Pascucci, and F. Charnley, *Handbook of the circular economy: Transitions and transformation*. Walter de Gruyter GmbH & Co KG, 2023.
- [14] J. Potting, M. P. Hekkert, E. Worrell, and A. Hanemaaijer, “Circular economy: Measuring innovation in the product chain,” 2017, policy report.
- [15] A. P. Velenturf and P. Purnell, “Principles for a sustainable circular economy,” *Sustainable Production and Consumption*, vol. 27, pp. 1437–1457, 2021.
- [16] N. O. Bonsu, “Towards a circular and low-carbon economy: Insights from the transitioning to electric vehicles and net zero economy,” *Journal of Cleaner Production*, vol. 256, p. 120659, 2020.
- [17] M. Yu, B. Bai, S. Xiong, and X. Liao, “Evaluating environmental impacts and economic performance of remanufacturing electric vehicle lithium-ion batteries,” *Journal of Cleaner Production*, vol. 321, p. 128935, 2021.
- [18] B. Marche, D. N. P. Rodriguez, O. Chéry, M. Camargo, and B. Christophe, “Comparison of manufacturing/remanufacturing CO₂ emissions balance: Application to a mowing machine,” in *2022 IEEE 28th International Conference on Engineering, Technology and Innovation (ICE/ITMC) & 31st International Association For Management of Technology (IAMOT) Joint Conference*. IEEE, 2022, pp. 1–7.
- [19] W. Zhou, J. Wang, P. Chen, C. Ji, Q. Kang, B. Lu, K. Li, J. Liu, and R. Ruan, “Bio-mitigation of carbon dioxide using microalgal systems: Advances and perspectives,” *Renewable and Sustainable Energy Reviews*, vol. 76, pp. 1163–1175, 2017.
- [20] D. D.-W. Tsai, P. H. Chen, and R. Ramaraj, “The potential of carbon dioxide capture and sequestration with algae,” *Ecological Engineering*, vol. 98, pp. 17–23, 2017.
- [21] P. Pereira, F. Wang, M. Inacio, M. Kalinauskas, K. Bogdzevič, I. Bogunovic, W. Zhao, and D. Barcelo, “Nature-based solutions for carbon sequestration in urban environments,” *Current Opinion in Environmental Science & Health*, vol. 37, p. 100536, 2024.
- [22] E. S. Rubin, H. Mantripragada, A. Marks, P. Versteeg, and J. Kitchin, “The outlook for improved carbon capture technology,” *Progress in Energy and Combustion Science*, vol. 38, no. 5, pp. 630–671, 2012.
- [23] T. Wilberforce, A. Olabi, E. T. Sayed, K. Elsaid, and M. A. Abdelkareem, “Progress in carbon capture technologies,” *Science of The Total Environment*, vol. 761, p. 143203, 2021.
- [24] V. Romano, G. Proietti, R. J. Pawar, and S. Bigi, “Evaluation of fracture network efficiency to CO₂ storage with a DFN approach,” *International Journal of Greenhouse Gas Control*, vol. 141, p. 104317, 2025.
- [25] L. Gratani, L. Varone, and A. Bonito, “Carbon sequestration of four urban parks in Rome,” *Urban Forestry & Urban Greening*, vol. 19, pp. 184–193, 2016.
- [26] Y. Yang, S. Tang, and J. P. Chen, “Carbon capture and utilization by algae with high concentration CO₂ or bicarbonate as carbon source,” *Science of The Total Environment*, vol. 918, p. 170325, 2024.
- [27] S. G. Nersesov, W. M. Haddad, and V. Chellaboina, “Optimal fixed-structure control for linear non-negative dynamical systems,” *International Journal of Robust and Nonlinear Control*, vol. 14, no. 5, pp. 487–511, 2004.
- [28] A. Ilka and N. Murgovski, “Novel results on output-feedback LQR design,” *IEEE Transactions on Automatic Control*, vol. 68, no. 9, pp. 5187–5200, 2022.
- [29] A. Bemporad, M. Morari, V. Dua, and E. N. Pistikopoulos, “The explicit linear quadratic regulator for constrained systems,” *Automatica*, vol. 38, no. 1, pp. 3–20, 2002.
- [30] L. Shi, Y. Yuan, and J. Chen, “Finite horizon LQR control with limited controller-system communication,” *IEEE Transactions on Automatic Control*, vol. 58, no. 7, pp. 1835–1841, 2012.
- [31] H. Maghfiroh, M. Nizam, M. Anwar, and A. Ma’Arif, “Improved LQR control using PSO optimization and Kalman filter estimator,” *IEEE Access*, vol. 10, pp. 18 330–18 337, 2022.
- [32] H. Jaleel and J. S. Shamma, “Design of real-time implementable distributed suboptimal control: An LQR perspective,” *IEEE Transactions on Control of Network Systems*, vol. 5, no. 4, pp. 1717–1728, 2017.
- [33] P. Duan, L. He, Z. Duan, and L. Shi, “Distributed cooperative LQR design for multi-input linear systems,” *IEEE Transactions on Control of Network Systems*, vol. 10, no. 2, pp. 680–692, 2022.
- [34] S. Gao and P. E. Caines, “Subspace decomposition for graphon LQR: Applications to VLSNs of harmonic oscillators,” *IEEE Transactions on Control of Network Systems*, vol. 8, no. 2, pp. 576–586, 2021.
- [35] S. J. Chacko, P. Neeraj, and R. J. Abraham, “Optimizing LQR controllers: A comparative study,” *Results in Control and Optimization*, vol. 14, p. 100387, 2024.
- [36] D. Masti, M. Zanon, and A. Bemporad, “Tuning LQR controllers: A sensitivity-based approach,” *IEEE Control Systems Letters*, vol. 6, pp. 932–937, 2021.
- [37] W. Levine and M. Athans, “On the determination of the optimal constant output feedback gains for linear multivariable systems,” *IEEE Transactions on Automatic Control*, vol. 15, no. 1, pp. 44–48, 2003.
- [38] H. Wang, H. Zhang, and M. Z. Chen, “Filter-expanded linear quadratic regulator and its application in wind turbine vibration control,” *IEEE Transactions on Control Systems Technology*, vol. 32, no. 5, pp. 1827–1838, 2024.
- [39] N. Arab, H. Vahedi, and K. Al-Haddad, “LQR control of single-phase grid-tied PUC5 inverter with LCL filter,” *IEEE Transactions on Industrial Electronics*, vol. 67, no. 1, pp. 297–307, 2019.
- [40] F. Zocco, P. Sopasakis, B. Smyth, and W. M. Haddad, “Thermodynamical material networks for modeling, planning, and control of circular material flows,” *International Journal of Sustainable Engineering*, vol. 16, no. 1, pp. 1–14, 2023.
- [41] F. Zocco, D. R. Lake, S. McLoone, and S. Rahimifard, “Synchronized object detection for autonomous sorting, mapping, and quantification of materials in circular healthcare,” *IEEE Transactions on Instrumentation and Measurement*, vol. 74, p. 5505110, 2025.
- [42] F. Zocco, A. Corti, and M. Malvezzi, “CIRL: Open-source environments for reinforcement learning in circular economy and net zero,” *arXiv preprint arXiv:2505.21536*, 2025.
- [43] F. Zocco, “Circularity of thermodynamical material networks: Indicators, examples, and algorithms,” *arXiv preprint arXiv:2209.15051*, 2024.
- [44] F. Zocco and M. Malvezzi, “Circular economy design through system dynamics modeling,” in *International Workshop IFToMM for Sustainable Development Goals*. Springer, 2025, pp. 530–538.

- [45] United Nations Climate Change, “The Paris agreement,” last access: 25 July 2025. Available at: <https://unfccc.int/process-and-meetings/the-paris-agreement>.
- [46] European Commission, “Critical raw materials,” , last access: 25 July 2025. Available at: https://single-market-economy.ec.europa.eu/sectors/raw-materials/areas-specific-interest/critical-raw-materials_en.
- [47] National Aeronautics and Space Administration (NASA), “NASA spacecraft maps Earth’s global emissivity,” last access: 25 July 2025. Available at: <https://www.jpl.nasa.gov/images/pia18833-nasa-spacecraft-maps-earths-global-emissivity/>.
- [48] S. Fuller, B. Greiner, J. Moore, R. Murray, R. van Paassen, and R. Yorke, “The Python control systems library (python-control),” in *2021 60th IEEE Conference on Decision and Control (CDC)*. IEEE, 2021, pp. 4875–4881.
- [49] R. L. Williams and D. A. Lawrence, *Linear state-space control systems*. John Wiley & Sons, 2007.